Insights into the hierarchical structure and digestion rate of alkali-modulated starches with different amylose contents

Dongling Qiao[1,2,3], Long Yu[1,2*], Hongsheng Liu[1], Wei Zou[4], Fengwei Xie[5,6**], George Simon[2], Eustathios Petinakis[3], Zhiqi Shen[3], Ling Chen[1]

[1] CPFRR, College of Food Science and Engineering, South China University of Technology, Guangzhou, Guangdong 510640, China

[2] Department of Materials Engineering, Monash University, Melbourne, Vic 3168, Australia

[3] CSIRO, Manufacturing, Melbourne, Vic 3168, Australia

[4] Centre for Nutrition and Food Sciences, Queensland Alliance for Agriculture and Food Innovation, The University of Queensland, Brisbane, Qld 4072, Australia

[5] Australian Institute for Bioengineering and Nanotechnology, The University of Queensland, Brisbane, Qld 4072, Australia

[6] School of Chemical Engineering, The University of Queensland, Brisbane, Qld 4072, Australia

[*] Corresponding author. Tel.: +86-20-87111971; E-mail: felyu@scut.edu.cn (L. Yu).

[**] Corresponding author. Tel.: +61 7 3346 3199; fax: +61 7 3346 3973; Email address: f.xie@uq.edu.au; fwhsieh@gmail.com (F. Xie).

Abstract: Combined analytical techniques were used to explore the effects of alkali treatment on the multi-scale structure and digestion behavior of starches with different amylose/amylopectin ratios. Alkali treatment disrupted the amorphous matrix, and partial lamellae and crystallites, which weakened starch molecular packing and eventually enhanced the susceptibility of starch to alkali. Stronger alkali treatment (0.5% w/w) made this effect more prominent and even transformed the dual-phase digestion of starch into a triple-phase pattern. Compared with high-amylose starch, regular maize starch, which possesses some unique structure characteristics typically as pores and crystallite weak points, showed evident changes of hierarchical structure and in digestion rate. Thus, alkali treatment has been demonstrated as a simple method to modulate starch hierarchical structure and thus to realize the rational development of starch-based food products with desired digestibility.

Keywords: Starch; Alkali treatment; In vitro digestion; Multi-scale structure; Amylose/amylopectin ratio

Chemical compounds studied in this article: Starch (PubChem CID: 24836924); Water (PubChem CID: 962); Sodium hydroxide (PubChem CID: 14798); Sodium azide (PubChem CID: 33557); Ethanol (PubChem CID: 702); 4-Hydroxybenzhydrazide (PubChem CID: 1742); Maltose (PubChem CID: 10991489)

1. Introduction

Starch is the main storage carbohydrate in most higher plants and is one of the most important energy sources for humans and animals. Starch contains two D-glucan biopolymers, *i.e.*, amylose, a relatively linear 1,4-α-D-glucan with a small number of long branches; and amylopectin, mainly a 1,4-α-D-glucan containing high-density branches (*ca.* 5% of glycosidic bonds are α-1,6) (Zhang et al., 2014a). These two macromolecules are organized on different length scales in the starch granule to form the supramolecular structure of starch, from the whole granule (<1 μm–100 μm), growth ring (100–400 nm), semi-crystalline lamellae (9–10 nm), to crystalline structure (>0.1 nm–*ca.* 1 nm) (Pikus, 2005; Zhang, Li, Liu, Xie & Chen, 2013). In addition, depending on the packing of amylopectin side chains into double helices and amylose single helices, the crystalline structure (polymorph) of starch has been classified as A-, B-, C- or V-type. All this multi-scale structure of starch depends on the botanical origin.

In addition, starch structure may be altered by various treatments, resulting in changes in the digestibility and other properties of starch. As a main food ingredient, starch is usually processed for consumption, in which case native starch in low-moisture foods (Blazek & Gilbert, 2010) (*e.g.*, biscuits and muesli), fruits, vegetables, and animal feeds can be ingested directly. Since the digestibility of starch may be associated with metabolic diseases such as Type II diabetes, obesity, and cardiovascular diseases, it plays a key role in determining the health benefits of starch-based foods (Zou, Sissons, Gidley, Gilbert & Warren, 2015). Hence, there has been huge interest in understanding the digestion behavior (reflected mainly by hydrolysis rate and digested proportion) of starch and starch-based foods, which is crucial for rational development of starch-based food products with desirable digestibility.

The Englyst method (Englyst, Kingman & Cummings, 1992) is extensively employed to assess the *in vitro* digestibility of starch. It characterizes the proportion of starch digested within a certain time period, based on which starch can be classified into three different types, *i.e.*, rapidly-digestible starch (RDS), slowly-digestible starch (SDS), and resistant starch (RS). The digestion rate of starch is further characterized by the hydrolysis indices, equal to the areas under the digestibility curve between the start

and selected completion time points (Aravind, Sissons & Fellows, 2011; Butterworth, Warren, Grassby, Patel & Ellis, 2012; Edwards, Warren, Milligan, Butterworth & Ellis, 2014). Nonetheless, these methods cannot allow for a rigorous, quantitative comparison between digestion rates and digested proportions, and are incapable of quantifiably determining the digestion rate constant as starch digestion proceeds. To offset this limitation, a novel method, termed as a logarithm of the slope (LOS) plot,(Poulsen, Ruiter, Visser & Iversen, 2003) by modelling the hydrolytic process using first-order enzyme kinetic principles (Goñi, Garcia-Alonso & Saura-Calixto, 1997), has been applied to acquire the hydrolysis rate of starch. The LOS plot enhances the differences in starch digestion rate constant and visibly reveals the number of starch digestion steps throughout the whole enzymatic hydrolysis period. This method based on the LOS plot has been used to identify and quantify the digestion rates and digested proportions in purified starches, homogeneous foods, and edible starch-rich plant tissues (Edwards et al., 2014).

For the production of starch and starch-based food products, alkali treatment has been widely used. This treatment has not only been confirmed effective at isolating starches from agro-products with high yields and purity, especially for starch tightly associated with protein (Correia & Beirão-da-Costa, 2012; Han & Hamaker, 2002), it has also been used for preparation of diverse starch-based foods, such as tortillas, yellow alkaline noodles and dumplings (Campus-Baypoli, Rosas-Burgos, Torres-Chavez, Ramírez-Wong & Serna-Saldivar, 1999; Lai, Karim, Norziah & Seow, 2002). Moreover, the treatment with reagents such as sodium hydroxide and sodium carbonate often imparts the foods with a characteristic aroma and flavor, as well as a firm and elastic texture (Karim et al., 2008). Therefore, it is necessary to understand how alkali treatment changes the structure and digestion behavior of starch.

Alkali treatment has been shown capable of altering the structures (morphology(Cai et al., 2014; Cardoso, Putaux, Samios & da Silveira, 2007; Jiang et al., 2014; Nadiha, Fazilah, Bhat & Karim, 2010; Paredes-Lópezb & Bello-Péreza, 2007; Wang & Copeland, 2012; Wang et al., 2014), short- and long-range orders (Cai et al., 2014; Cardoso et al., 2007; Jiang et al., 2014; Wang & Copeland, 2012), and semi-crystalline lamellae (Cai et al., 2014)) and properties (*e.g.*, swelling(Jiang et al., 2014; Paredes-Lópezb & Bello-Péreza, 2007; Wang & Copeland, 2012; Wang et al., 2014), solubility (Jiang et al.,

2014; Paredes-Lópezb & Bello-Péreza, 2007; Wang et al., 2014), pasting(Han & Tyler, 2003; Karim et al., 2008; Lai et al., 2002; Nadiha et al., 2010; Nor Nadiha, Fazilah, Bhat & Karim, 2010; Wang, Li, Wang, Liu & Adhikari, 2012), rheological (Shiau & Yeh, 2001), and thermal properties (Cai et al., 2014; Cardoso et al., 2007; Lai et al., 2002; Nadiha et al., 2010; Paredes-Lópezb & Bello-Péreza, 2007; Wang & Copeland, 2012; Wang et al., 2014)) of starches of various botanical origins (*e.g.*, corn (Paredes-Lópezb & Bello-Péreza, 2007; Wang et al., 2012) rice,(Cai et al., 2014; Cardoso et al., 2007), potato (Nadiha et al., 2010), sago (Karim et al., 2008), and pea (Han & Tyler, 2003; Wang & Copeland, 2012)).. However, the effect of alkali treatment on the digestion behavior has not been extensively studied as on other properties of starch. To date, only the changes in *in vitro* digestibility of alkali-treated starches, based on the Englyst classification method, have been investigated, which has shown that alkali treatment can increase the digested proportion (Wang & Copeland, 2012; Wang et al., 2014). Yet, alkali-induced changes in digestion rate of starch have not been understood, in particular from a hierarchical structural view. The lack of this understanding prevents us from exploring the mechanism of how alkali treatment changes the digestion behavior of starch and the rational application of alkali-treated starch for desired digestion patterns.

Although strong alkali can quickly disrupt starch structure, the degradation of starch molecules is often induced (Han & Lim, 2004), due to the β-elimination of reducing semiacetal groups. Considering this fact, low alkali concentrations (e.g., 0.1%, 0.2%, and 0.4%), moderate temperatures (e.g., 30 °C and 35 °C) and long time periods (up to 30 days) (Cai et al., 2014; Jiang et al., 2014; Nadiha et al., 2010; Praznik, Buksa, Ziobro, Gambuś & Nowotna, 2012; Wang & Copeland, 2012) have been widely used for a slow disruption of starch supramolecular structure without molecular degradation. This study is mainly focused on how the starch supramolecular hierarchical structure and alkali treatment affect the digestion behavior of starch. Thus, moderate alkali treatment for long periods should be used in the present work, although further investigations are still needed to reduce the treatment time and thus to better meet practical requirements

On the other hand, starches of different origins can have different amylose contents (up to 85%). The

amylose content has a prominent influence on starch hierarchical structure. In particular, while regular starches (with 10–30% amylose content) normally contain a large amount of A-type crystallites, high-amylose starches (with >50% amylose content) usually exhibit a B-type polymorph with lower crystallinity and are less susceptible to various physicochemical treatments such as acid hydrolysis and hydrothermal treatment (Kim & Huber, 2010; Zhang et al., 2014a). Thus, starches with different amylose contents can be ideal models to probe the alkali treatment-digestion mechanism. Regarding this, the current work involved the use of regular and high-amylose maize starches to study the effect of mild alkali on the lamellar and crystalline structures of starch as well as thermal and digestion behaviors (especially digestion rate). This resulted in ultimate understanding of the chemistry/structure-digestibility relationship for alkali-treated starch. More importantly, the understanding from this work could be helpful in developing starch-based products with tailored digestibility using alkali and more similar chemical treatments.

2. Materials and Methods

2.1 Materials

Regular maize starch (RMS) and high-amylose maize starch (Gelose 50 or G50) were purchased from Penford Australia Pty Ltd. (Lane Cove, NSW, Australia). RMS and G50 have amylose/amylopectin ratios of 23/77 and 50/50, respectively, as measured using the iodine colorimetric method (Tan, Flanagan, Halley, Whittaker & Gidley, 2007). The moisture content of each starch sample was determined using a MA35 moisture analyzer (Sartorius Stedim Biotech GmbH, Germany). Sodium hydroxide, sodium azide, and ethanol, purchased from Tianjin Kemeou Chemical Reagent Co., Ltd. (China), were of analytical grade. α-Amylase from porcine pancreas (A-3176; 23 unit amylase/mg solid, one unit liberates 1.0 mg of maltose from starch in 3 min at pH 6.9 at 37 °C), phosphate buffered saline tablet (P4417-100TAB), 4-hydroxybenzhydrazide (PAHBAH, H9882) and maltose (M-9171) were supplied by Sigma-Aldrich Pty Ltd. (Castle Hill, NSW, Australia).

2.2 Preparation of alkali-treated starch

About 10.0 g of starch was added into 150 mL sodium hydroxide aqueous solution at a concentration of 0.1% (w/v) or 0.5% (w/v) with 0.1% (w/v) sodium azide as a chemical preservative. The starch slurries were kept at 35 °C for 6 or 12 days with intermittent shaking twice a day for several minutes to fully re-suspend the starch. After the treatment, the starch sediment was washed with 95% ethanol (Jiang et al., 2014; Wang & Copeland, 2012) and centrifuged for 3–5 times until the slurry became neutral. Then, the starch sediment was dried in an oven at 35 °C for 48 h. In the following discussion, the samples are coded in the format of "RMS-0.5%-12", where "RMS" denotes the type of starch, "0.5%" indicates the concentration of sodium hydroxide, and "12" means the days for treatment.

2.3 Synchrotron small-angle X-ray scattering (SAXS)

SAXS measurements were performed on the SAXS/WAXS beamline (flux, 1013 photons/s) at the Australian Synchrotron (Clayton, Vic, Australia), at a wavelength λ = 1.47 Å. A Pilatus 1M camera (active area 169 × 179 mm; and pixel size 172 × 172 μm) was used to record the 2D scattering patterns. The one-dimensional (1D) data were obtained from the 2D scattering patterns using the scatterBrain software, and the data in the angular range of $0.0015 < q < 0.15$ Å^{-1} were used as the SAXS pattern, where $q = 4\pi\sin\theta/\lambda$ (where 2θ is the scattering angle and λ the X-ray wavelength). All the data were background subtracted and normalized. Starch slurries with a starch concentration of 40 wt% were prepared by adding a desired amount of water to the starch samples. The starch suspensions were placed on a multi-well stage provided by the Australian Synchrotron, and then the SAXS data were recorded for an acquisition time of 1 s. The scattering of pure water with a Kapton tape (5413 AMBER 3/4IN X 36YD, 3M, USA) on the stage window was used as the background data.

2.4 X-ray diffraction (XRD)

Before the measurements, the unmodified and alkali-treated starch samples were kept in an oven at 35 °C for 12 h. The starch samples displayed similar moisture content of approx. 11%. The crystalline structure of starch samples was evaluated using a powder X-ray diffractometer (D8 Advance, Bruker AXS Inc., Madison, WI, USA) equipped with a graphite monochromator, a copper target and a

scintillation counter detector. The radiation parameters were 40 kV and 30 mA, with a slit of 2 mm. XRD patterns were acquired for a 2θ range of 4–40°, with a step size of 0.02° and a step rate of 0.5 s per step. The relative crystallinity (X_c, %) for the starch samples was calculated using the PeakFit software (Ver. 4.12), according to Eq. (1):

$$X_c = \frac{\sum_{i=1}^{n} A_{ci}}{A_t} \quad (1)$$

in which, A_{ci} is the area under each crystalline peak with index i, and A_t is the total area of the diffraction pattern.

2.5 Differential scanning calorimetry (DSC)

The thermal behaviors of native and alkali-treated starches were measured using a PerkinElmer DSC 8500 with nitrogen purge gas (Liu, Yu, Xie & Chen, 2006; Zhang et al., 2013). A high-pressure stainless steel pan with a gold-plated copper seal was used to run the tests. The starch samples with 70% moisture content were prepared by premixing the starches with distilled water in sealed glass vials, which were then kept at 26 °C for 12 h before the measurement to achieve homogeneous samples. The samples (*ca.* 12-15 mg) were heated from 30 °C to 120 °C at a heating rate of 10 K/min. The gelatinization onset temperature (T_o) and enthalpy (ΔH) for the starch samples were recorded. All results were reported as averages of three replicates.

2.6 In vitro digestion

In vitro digestion of starch was carried out in duplicate. A centrifuge tube with 90.0 mg of dried starch and 16.0 mL of deionized water was incubated at 37 °C. Then, 5.0 mL of phosphate buffer solution (PBS; one phosphate buffered saline tablet dissolved in 200 mL of deionized water yields 0.01 M phosphate buffer, 0.0027 M potassium chloride and 0.137 M sodium chloride, pH 7.4, at 25°C) with 9.0 mg of porcine α-amylase was pipetted into the tube. Afterwards, 100.0 μL of the digestion solution was collected at each time point and transferred into a prepared centrifuge tube containing 900.0 μL of 0.3 mol/L Na_2CO_3 solution to terminate enzymatic digestion. The 1.0 mL of mixed solution was then centrifuged at 8000 *g* for 10 min, before 100.0 μL of supernatant was pipetted into 1.0 mL of PAHBAH

solution (prepared by dissolving 500.0 mg of PAHBAH powder into 10.0 mL of 0.5 M HCl, followed by addition of 90.0 mL of 0.5 M NaOH). The resulting solution was incubated in boiling water for 5 min. After cooling to ambient temperature, the absorbance at 410 nm (McDougall et al., 2005; Nwosu et al., 2011) was recorded by using a UV-1700 spectrophotometer (Shimadzu Corp., Kyoto, Japan). Maltose solution (1.0 mol/L) was referenced for quantifying starch digested. The percentages of the starch digested were calculated according to Eq.(2):

$$\mathrm{SD}(\%) = A_{sample} \times \frac{100\mu L \times 1.0 mg/L}{A_{maltose}} \times 10 \times 210 \times \frac{100\%}{90mg} \times \frac{324}{342} \quad (2)$$

In this equation, *SD* is the percentage of starch digested, and A_{sample} and A_{maltose} are the absorbances for starch digestion solution and maltose standard, respectively. The value of 10 × 210 is the computational multiple from 100.0 μL aliquots to 21.0 mL reaction solution, and 324/342 is the transformation coefficient from maltose to starch in weight.

2.7 First-order kinetics

Except the commonly-used first-order kinetic model (Eq.(3)), the accompanying logarithm of the slop (LOS) plot (Eq.(4)) was adopted to fit the digestion data to describe the sequential first-order kinetics of starch digestion (Zou et al., 2015).

$$C_t = C_\infty(1 - e^{-k \cdot t}) \quad (3)$$

$$\ln \frac{dC_t}{dt} = -k \cdot t + \ln(C_\infty \cdot k) \quad (4)$$

where C_t (%) is the amount of starch digested at a given time (t (min)), C_∞ (%) is the estimated percentage of starch digested at the end point of a digestion stage, and k (min^{-1}) is the coefficient of starch digestion rate. The calculated digestion data ($ln[(C_{i+2} - C_i)/(t_{i+2} - t_i)]$) at each time point ($(t_{i+2} + t_i)/2$), except the last two points, was used to obtain the LOS pattern and the related fit curve.

The LOS plot visibly reveals the number of starch digestion steps throughout the whole reaction period according to the changes in the slope of digestion pattern ($ln(dC_t/dt)$) versus the time (t). Therefore, using the LOS plot derived from digestion data, the different digestion stages with different digestion rate coefficients (k) could be shown. The obtained k and C_∞ were employed to plot the starch

digestion curve according to Eq.(3) to compare the original data with the fit starch digestion curves generated by the fit model.

2.8 Statistical analysis

Data were expressed as means ± standard deviations (SD). Starch digestion rate constants were analyzed by one-way ANOVA and multiple comparison test with least significant difference using IBM SPSS software version 20.0 (Chicago, IL, USA). A statistical difference of $P < 0.05$ was considered to be significant. Linear regression fitting and regression analysis were carried out in Microsoft Excel 2010 (Redmond, WA, USA).

3. Results and Discussion

3.1 Lamellar structure

Fig. 1 shows the double logarithm SAXS patterns of native and alkali-treated starches in the range of $0.015\ Å^{-1} < q < 0.15\ Å^{-1}$. All starch samples displayed a scattering peak at *ca.* $0.06\ Å^{-1}$, corresponding to the average repeat distance of semi-crystalline lamellae (crystalline-amorphous lamellae) of starch (Zhang et al., 2015). Normally, semi-crystalline lamellae with a high degree of ordering and without flawless can generate a scattering peak with fine visibility (Zhang et al., 2014b). As revealed by the SAXS patterns in Fig. 1, alkali treatment reduced the visibility of the lamellar peak at *ca.* $0.06\ Å^{-1}$, indicating an increased amount of flawed semi-crystalline lamellae with a lower ordering degree. That is, for both RMS and G50, alkali treatment disrupted semi-crystalline lamellae to a certain degree and decreased the organization of lamellae.

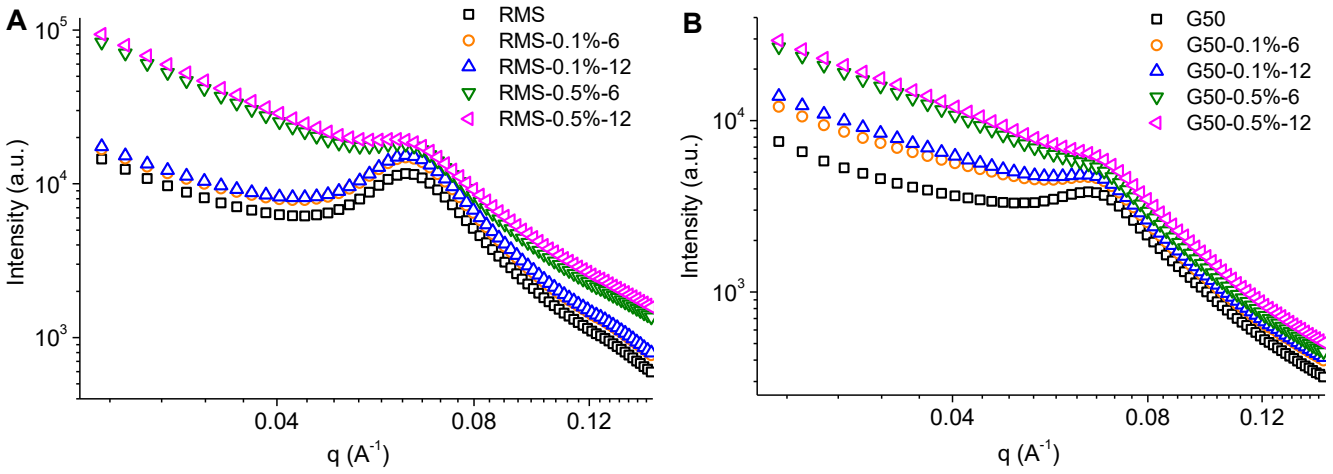

Fig.1 SAXS patterns for native and alkali-treated RMS and G50.

Apart from the reduced visibility of lamellar peak, the scattering intensity at low q values was also raised by alkali treatment (see Fig. 1), which could be attributed to the changes in the lamellar regions and the background materials on the nano scale (Zhang et al., 2013). According to the paracrystalline model (Cameron & Donald, 1992, 1993a, b), two parameters on semi-crystalline lamellae could be acquired, *i.e.*, the electron density difference between crystalline and amorphous lamellae $\Delta\rho = \rho_c - \rho_a$ (where ρ_c and ρ_a are the electron densities of crystalline lamellae and amorphous lamellae in semi-crystalline lamellae, respectively) and the electron density difference between the amorphous background and amorphous lamellae $\Delta\rho_u = \rho_u - \rho_a$ (where ρ_u is the electron density of the amorphous background (amorphous growth rings)). While the major effect of increasing $\Delta\rho$ is to increase the overall intensity, the increase in $\Delta\rho_u$ has the concurrent effects of raising the low-angle intensity and lowering the definition of the peak without changing the peak position (Cameron & Donald, 1992). From Fig. 1, compared to the native counterparts, increases in the overall scattering intensity and in the low-angle intensity and a decrease in the peak definition were observed for alkali-treated RMS and G50, and this phenomenon became more apparent especially as the alkali concentration (not treatment time) increased. This indicates that alkali treatment increased both $\Delta\rho$ and $\Delta\rho_u$, resulting from a greater destruction to amorphous lamellae, and relatively lower destruction to the amorphous background and

crystalline lamellae. Nonetheless, previous reports confirmed that alkali treatment could reduce not only the value of $\Delta\rho_u$ for *Araucaria angustifolia* starch (Thys et al., 2008) but also the value of $\Delta\rho$ for *indica* and high-amylose rice starches (Cai et al., 2014).

To further illustrate the alterations of semi-crystalline lamellae induced by alkali treatment, the average thicknesses of semi-crystalline (d), crystalline (d_c) and amorphous (d_a) lamellae were obtained using the linear correlation function $f(r)$ (Zhang et al., 2015), as shown in Eq. (5):

$$f(r) = \frac{\int_0^\infty I(q)q^2 \cos(qr)dq}{\int_0^\infty I(q)q^2 dq} \quad (5)$$

In this equation, r(nm) is the distance in real space, and d is the second maximum of $f(r)$ (the repeat distance, *i.e.*, the thickness of semi-crystalline lamellae). d_a, representing the average thickness of amorphous lamellae within semi-crystalline lamellae, can be acquired by the solution of the linear region and the flat $f(r)$ minimum. Thus, d_c, the average thickness of crystalline lamellae within the semi-crystalline lamellae, is calculated by $d_c = d – d_a$.

The calculated lamellar parameters are summarized in Table 1. The thickness of semi-crystalline lamellae kept constant for RMS after the 0.1% concentration alkali treatment, whereas for G50 this thickness slightly increased but no further changes with time was observed. Nonetheless, the high concentration (0.5%) alkali solution resulted in a similar increase in the thickness of semi-crystalline for both RMS and G50. Hence, unlike previous findings (Cai et al., 2014; Thys et al., 2008) that alkali treatment makes semi-crystalline lamellae thinner for C-polymorphic *Araucaria angustifolia* starch (a hybrid of A- and B-polymorphs) but does not alter the thickness of semi-crystalline lamellae for A- and C-polymorphic rice starches, the results here demonstrated that alkali tended to increase the semi-crystalline lamellar thickness for maize starches with a single A- or B-polymorph.

Table 1. Lamellar, crystalline and thermal parameters of native and alkali treated starches [a]

	native	0.1% NaOH	0.5% NaOH

		starch	6 days	12 days	6 days	12 days
RMS	d (nm)	9.35±0.00	9.35±0.00	9.35±0.00	9.55±0.00	9.57±0.01
	d_a (nm)	2.65±0.01	2.64±0.00	2.64±0.01	2.60±0.01	2.58±0.01
	d_c (nm)	6.70±0.01	6.71±0.00	6.71±0.01	6.95±0.01	6.99±0.02
	X_c (%)	39.80	38.54	37.11	36.57	36.34
	ΔH (J/g)	14.67±0.15	14.47±0.32	14.07±0.27	8.33±0.32	8.27±0.47
	T_o (°C)	68.37±0.28	70.11±0.16	69.32±0.34	77.12±0.28	77.20±0.39
G50	d (nm)	9.40±0.00	9.47±0.00	9.47±0.01	9.62±0.00	9.62±0.01
	d_a (nm)	2.57±0.01	2.58±0.01	2.58±0.01	2.65±0.01	2.65±0.01
	d_c (nm)	6.83±0.01	6.89±0.01	6.89±0.02	6.97±0.01	6.97±0.02
	X_c (%)	32.68	32.41	31.05	31.22	31.16
	ΔH (J/g)	6.88±0.47	6.22±0.38	6.86±0.39	5.52±0.25	4.96±0.39
	T_o (°C)	73.94±0.20	73.70±0.12	73.64±0.38	78.93±0.30	79.18±0.01

[a] Parameters measured by SAXS: d, average thickness of semi-crystalline lamellae; d_c, average thickness of crystalline lamellae; d_a, average thickness of amorphous lamellae. Parameter obtained by XRD: X_c, relative degree of crystallinity. Parameters of endotherm G measured by DSC: ΔH, enthalpy; T_o, onsite temperature.

For clarifying how the thickness of semi-crystalline lamellae was increased by alkali, the evolution for the thicknesses of crystalline and amorphous lamellae was also examined. From the d_c and d_a results in Table 1, it is seen that after the alkali treatment (especially 0.5%), an increase in the thickness of crystalline lamellae and a decrease in the thickness of amorphous lamellae could be observed for RMS, whereas for G50 the treatment (in particular 0.5%) increased the thicknesses of both crystalline and amorphous lamellae. This suggested that alkali treatment could make semi-crystalline lamellae (d) thicker by increasing the thickness of crystalline lamellae (d_c) rather than that of amorphous lamellae (d_a) for RMS, and by simultaneously increasing both the thicknesses of crystalline (d_c) and amorphous (d_a) lamellae for G50. Accounting for this, alkali ions penetrated into the starch granule interior to partially break the hydrogen bonding network of starch crystallites, leading to movement of double helices in crystalline lamellae and thus an increase in semi-crystalline lamellae. In addition, it is noted that alkali treatment led to out-phasing of starch molecules from amorphous lamellae of RMS and thus reduced the

297 amorphous lamellar thickness, whereas for G50 the treatment tended to increase the thickness of
298 amorphous lamellae, presumably due to alkali-induced swelling in amorphous lamellae (rather than the
299 predominantly out-phasing of starch molecules) or disorganization of partial crystalline lamellae (i.e.,
300 transformation of crystalline lamellae into amorphous lamellae). This was again different from the case
301 for *Araucaria angustifolia* starch (Thys et al., 2008) which showed alkali decreased the thickness of
302 amorphous lamellae but did not apparently change that of crystalline lamellae.
303 *3.2 Crystalline structure*
304 Since the starch granule is a semi-crystalline system comprised of crystalline and amorphous regions,
305 the XRD pattern of starch shows sharp peaks for the crystalline regions and a diffuse pattern for the
306 amorphous components. Fig. 2 shows the XRD patterns of RMS and G50 before and after alkali
307 treatment. While RMS displayed a typical A-type polymorph with intense diffraction peaks at *ca.* 15°
308 and 23° (2θ), and an unresolved doublet at *ca.* 17° and 18°; G50 exhibited a typical B-type polymorph
309 with the strongest diffraction peak at around 17°, several smaller peaks at *ca.* 15°, 20°, 22° and 24°, and
310 a characteristic peak at *ca.* 5.6°. For both starches, alkali treatment (with increased alkali concentration
311 and treatment time) resulted in no change to the original polymorphic type, which was in agreement with
312 previous findings (Cai et al., 2014; Cardoso et al., 2007; Jiang et al., 2014; Wang & Copeland, 2012).
313
314

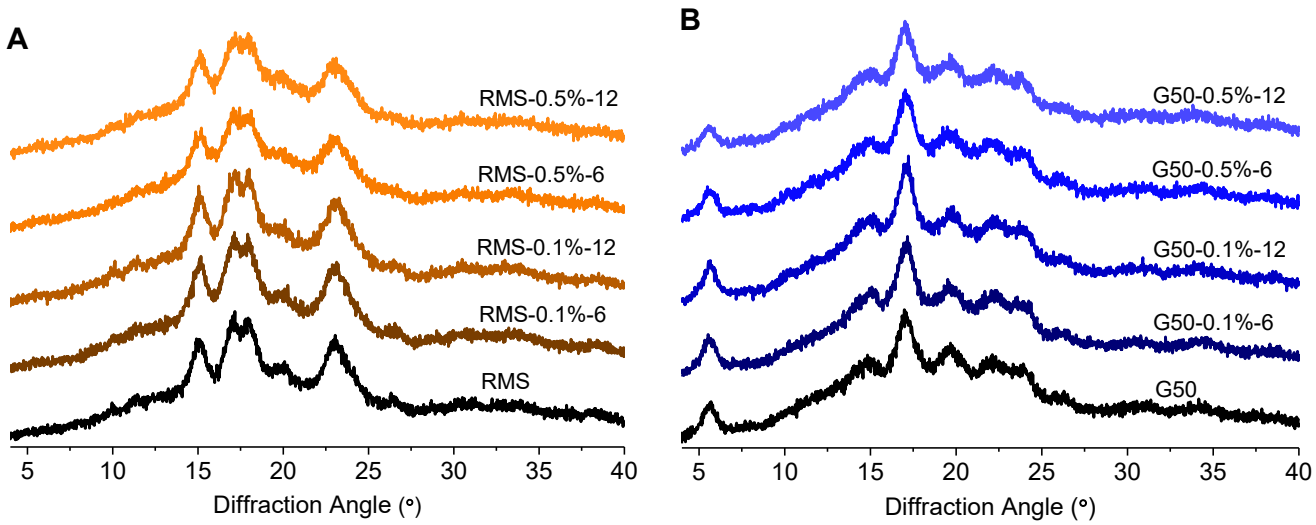

Fig. 2 XRD patterns for native and alkali-treated RMS and G50.

The relative degree of crystallinity (X_c) was calculated from the ratio of the total diffraction peak area to the total area of diffraction pattern, and the results are recorded in Table 1. Expectedly, RMS showed higher X_c than did G50. With a higher amylopectin content in RMS, amylopectin side chains formed double-helices (the short-range-scale order) and contributed to an increase in the quantity of starch crystallites (the long-range-scale order) (Manners, 1989; Tan et al., 2007). With alkali treatment, the crystallites were reduced. A greater decrease in X_c was observed for RMS, especially when a higher alkali concentration was used, suggesting that RMS crystallites were more susceptible to alkali treatment. Crystallinity reduction is normally observed for alkali treated starch (Cardoso et al., 2007; Thys et al., 2008; Wang & Copeland, 2012), though alkali probably increase the quantity of crystallites through preferentially attacking the amorphous region rather than the crystalline regions (Jiang et al., 2014).

The polymorphic components (crystallites) of starch at the long-range scale are predominantly comprised of monoclinic and/or hexagonal crystal units which are constituted by short-range double-helices and inter-helical water molecules. Those double-helices and water molecules are organized together through a huge amount of inter- and intra-molecular hydrogen bonds (Perez & Bertoft, 2010). Hence, the reduction of starch crystallites during alkali treatment was considered due to the breakage of

hydrogen bonds at the molecular level.

A previous study (Thys et al., 2008) has shown that for a C-polymorphic starch (*Araucaria angustifolia*), the B-type crystallites in the center of starch granule have greater susceptibility to alkali than do the more superficial A-type crystallites, due to the large quantity of water on the crystalline packing. Also, the crystallites of B-polymorphic starch (*D. persimilis*) are disrupted by alkali firstly with cavity formation, accompanied by the destruction of amorphous components in the latter stage, while for an A-type starch (*D. zingiberensis*) the crystallites are gradually degraded in the whole process as the compact structure and bulk crystalline lamellae form a protective layer around (Jiang et al., 2014). In this current work, however, with alkali treatment especially at high concentration (0.5%), RMS experienced a more pronounced increase in the average thickness of crystalline lamellae consisting of A-type double-helices. In other words, the alkali was more powerful at degrading the A-type crystallites of RMS than the B-type polymorph of G50. This information on how alkali reduces starch crystallinity is important in the following discussion about *in vitro* digestion.

3.3 Thermal behaviors

Fig. 3 presents the DSC thermograms of RMS and G50 before and after alkali treatment, and the related thermal parameters are summarized in Table 1. For native RMS and G50, two endotherms, termed as G and M2, were observed, attributed to the melting of amylopectin orders (crystallites and double-helices) and amylose-lipid complexes, respectively (Cooke & Gidley, 1992; Liu et al., 2006; Russell, 1987). Consistent with our previous report (Liu et al., 2006), G50 showed a lower enthalpy (ΔH) and a higher onset temperature (T_o) of the endotherm G than did RMS. This is presumably due to the fact that compared to G50, RMS contained inferior A-type crystallites with “weak points” resulting from short double helices and branch points clustered in the crystalline region (Jane, Wong & McPherson, 1997), which led to weaker thermal resistance of RMS amylopectin orders (i.e., a lower T_o of the endotherm G).

With alkali treatment, the endotherm M2 for both starches became less apparent, as the alkali induced the disassociation of amylose-lipid complexes. RMS showed a greater decrease in ΔH than G50,

which was similar to the trend of changes in crystallinity (X_c) (Table 1). Besides, an increase in G thermal transition temperature was observed for both RMS and G50, with RMS experiencing a more prominent increase in T_o. This effect was evidently enhanced by increasing the alkali concentration (rather than the treatment time). Along with the XRD results, the DSC results here revealed that although some starch crystallites were disorganized by alkali, leading to reduced X_c, the rearrangement of starch molecular chains occurred to allow the formation of new starch molecular orders (amylopectin crystallites and double-helices) with increased thermal stability (demonstrated by the increased thermal transition temperature). This was similar to the changes in crystallinity and thermal parameters of starch as induced by heat-moisture treatment (Hoover, 2010; Zhang et al., 2014b). As the alkali was more effective at changing the structural characteristics of RMS, the thermal stability of RMS orders showed a greater increase, caused by enhanced rearrangement of starch molecules.

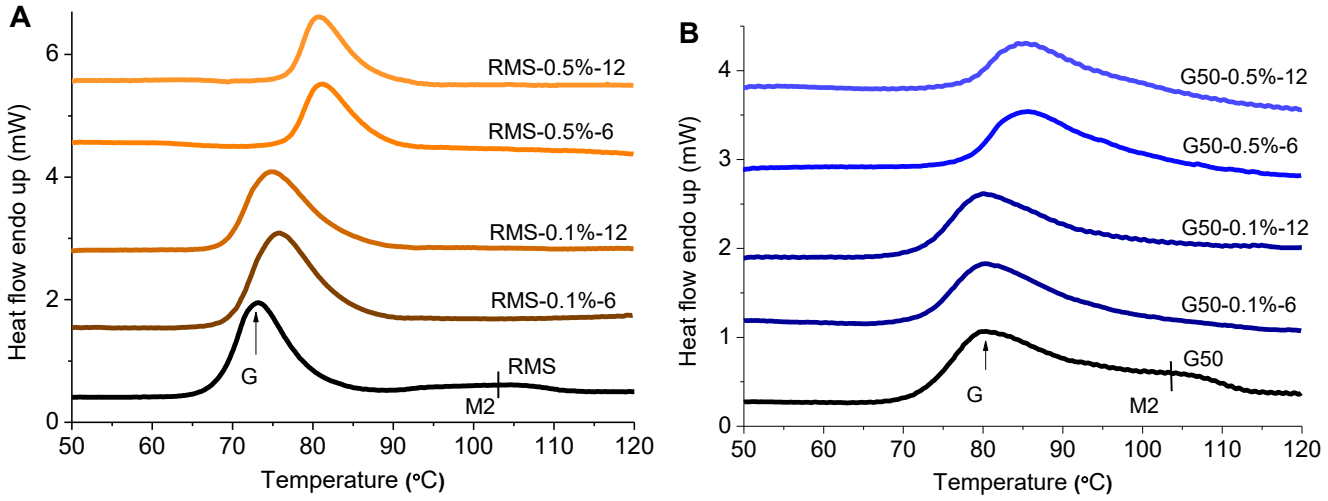

Fig. 3 DSC thermograms for native and alkali-treated RMS and G50.

3.4 Digestion rate of untreated starch

The typical digestion curves and LOS plots, along with their fit curves, for native RMS and G50 are

shown in Fig. 4; and Table 2 presents the related parameters of starch digestion. The LOS plots consisted of two linear ranges, identified by different rate constants (k_1 and k_2). This suggested that both starches experienced digestion in dual phases, with the first phase having a higher digestion rate than the second one ($k_1 > k_2$). For RMS, k_2 was just *ca.* ¼ of k_1; and for G50, k_2 was 1/13 of k_1 (Table 2).

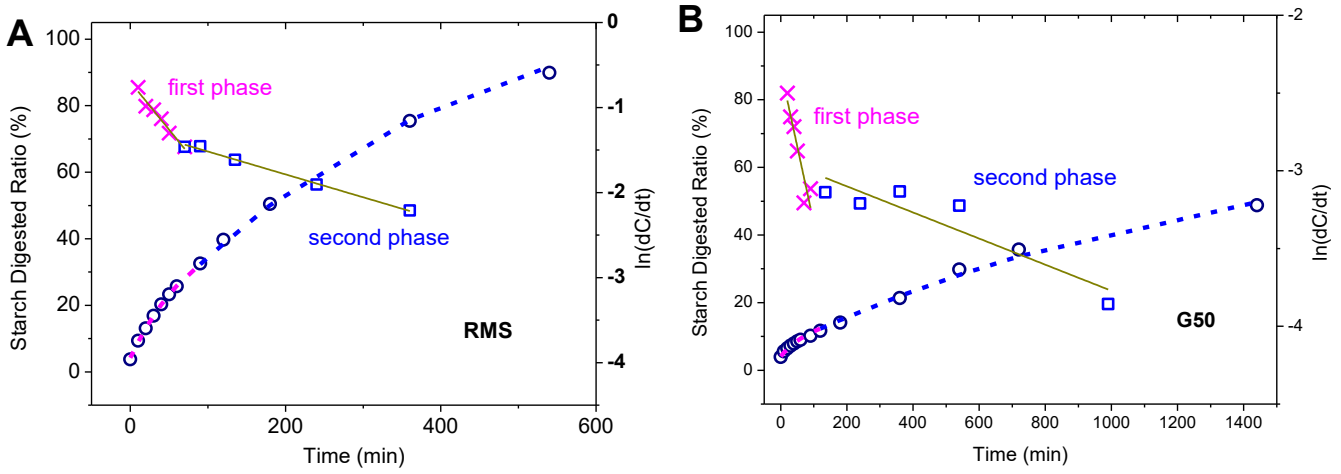

Fig. 4 Typical digestion curves, LOS plots and fit curves for native RMS and G50. ○, Experiment data; × and □, LOS plot data in first and second phases, respectively; ——, linear fit curve for LOS plot data; – – and – – , fit curve based on the slope and intercept values of the linear fit curve for LOS plot in first and second phases, respectively.

The dual-phase digestion for both starches could result from the heterogeneity of starch granules, in particular the semi-crystalline nature. As reported before (Gallant, Bouchet, Buléon & Pérez, 1992; Lopez-Rubio, Htoon & Gilbert, 2007), amorphous starch is more easily hydrolyzed by an enzyme due to the relatively loose packing of starch molecules, whereas starch molecules in long- and short-range orders are less accessible to the enzyme (digestible at a rather lower rate or even indigestible) unless they are disorganized. Here, it is proposed that in the first phase the digestion mainly occurred to amorphous starch at a higher digestion rate, although the present work did not show any difference in

399 the digestion rate between non-lamellar amorphous starch and lamellar amorphous starch.

400

401

402 **Table 2.** Digestion parameters of native and alkali-treated starches [a]

			native starch	0.1% NaOH 6 days	0.5% NaOH 6 days
RMS	Phase I	k_1 (min^{-1})	$(1.07\pm0.09)\times10^{-2}$	$(1.03\pm0.04)\times10^{-2}$	$(5.06\pm0.28)\times10^{-2}$
		t_1 *(min)*	90±0	90±0	50±0
		C_{t1} (%)	23.35±0.07	27.55±3.71	42.12±0.323
	Phase II	k_2 (min^{-1})	$(0.29\pm0.02)\times10^{-2}$	$(0.28\pm0.01)\times10^{-2}$	$(0.95\pm0.11)\times10^{-2}$
		t_2 *(min)*	540±0	540±0	180±0
		C_{t2} (%)	90.88±1.40	86.11±1.64	56.11±0.00
	Phase III	k_3 (min^{-1})	--	--	$(0.25\pm0.02)\times10^{-2}$
		t_3 *(min)*	--	--	540±0
		C_{t3} (%)	--	--	95.30±0.16
G50	Phase I	k_1 (min^{-1})	$(1.00\pm0.01)\times10^{-2}$	$(1.05\pm0.00)\times10^{-2}$	$(3.49\pm0.12)\times10^{-2}$
		t_1 *(min)*	120±0	120±0	60±0
		C_{t1} (%)	9.17±0.21	13.61±0.41	20.90±0.77
	Phase II	k_2 (min^{-1})	$(0.08\pm0.00)\times10^{-2}$	$(0.10\pm0.01)\times10^{-2}$	$(0.46\pm0.04)\times10^{-2}$
		t_2 *(min)*	1440±0	1440±0	360±0
		C_{t2} (%)	49.92±1.61	61.79±2.51	29.58±0.45
	Phase III	k_3 (min^{-1})	--	--	$(0.09\pm0.02)\times10^{-2}$
		t_3 *(min)*	--	--	1440±0
		C_{t3} (%)	--	--	69.81±3.99

403 [a] k_1, k_2 and k_3 are the rate constants for the first, second and third phases of digestion, respectively; t_1, t_2 and t_3 are
404 the times required for the first, second and third phases of digestion, respectively; C_{t1}, C_{t2} and C_{t3} are the digested
405 proportion of starch in the first, second and third phases of digestion, respectively.

406

407

408 While G50 and RMS had similar hydrolysis rates in the first phase (k_1), the latter had a greater
409 proportion of starch digested (C_{t1}). As shown in Table 2, C_{t1} was 23.35% for RMS and 9.17% for G50.
410 We also found that waxy maize starch (almost without amylose) had even higher C_{t1} but still with

similar k_1 (unpublished data). This means the fraction of starch that could be rapidly digested in the first phase was not only linked to the crystallinity, but also to other structural features as influenced by the amylose content. RMS was observed to have a large number of pores which could connect the granule surface to the interior (hilum), whereas G50 is known to have a compact granule structure without such pores (Chen et al., 2009) (see SEM images in Fig. S1). As the pores allowed the penetration of α-amylase molecules (with a size of *ca.* 6 nm) (Payan et al., 1980) into the interior of the granules, RMS could be digested centrifugally through an "inside-out" manner; in contrast, for G50, the absence of pores hindered the penetration of enzyme into the granules, resulting in a "centripetal" (from surface to core) digestion pattern (Dhital, Butardo, Jobling & Gidley, 2015; Zhang, Ao & Hamaker, 2006). Consequently, RMS had a large fraction of loosely-packed starch molecules in the hilum, close to the pores, and in the granule surface, which were all highly susceptible to the enzyme (and easily leached out from the starch granule) and could be rapidly hydrolyzed at a high rate (k_1). For G50, the enzyme could only rapidly digest some starch molecules in the granule surface and the leached molecules although at a similar high rate (k_1). In other words, while both RMS and G50 showed similar rates in the first digestion phase, the former had a higher digested proportion of starch (C_{t1}) at the end of this first phase.

In the second digestion phase, the enzyme gradually hydrolyzed the digestible matrix of remainder starch. At the end of the second phase, 90.88% (C_{t2}) of RMS and 49.92% (C_{t2}) of G50 were hydrolyzed. Since the amorphous content in RMS was 60.02% (Table 1), it is proposed that in the second phase, not only could the amorphous matrix in RMS be sufficiently digested by the enzyme, also part of A-type crystallites were hydrolyzed. Nevertheless, as G50 had an amorphous content of 67.32% (Table 1), only part of this amorphous starch was hydrolyzed by the enzyme. It is worth mentioning that the reduction of enzyme concentration and the deactivation of enzyme were unavoidable as starch digestion proceeds. Since our work mainly focused on the effects of starch inherent structure and alkali treatment on the digestion behavior of RMS and G50, those enzyme related factors would not be discussed in the following part.

Besides, RMS had much higher k_2 than G50 (*ca.* 2.5 times higher), suggesting that the remainder amorphous matrix of RMS after the first digestion phase could be digested more easily than that of G50. It was possible that for RMS the enzymatic hydrolysis in the first phase made the feature of pores more apparent and promoted the starch-enzyme interactions. Besides, compared with G50, RMS with A-type polymorph possesses shorter amylopectin side chains and a larger proportion of short chains (Hizukuri, 1985). While B- polymorphic G50 contains branch points mostly clustered in the amorphous regions, A-polymorphic RMS has branch points scattered in both amorphous and crystalline regions. The shorter double helices derived from the shorter side chains and the branch linkages presented in the crystalline region lead to the "weak points" (i.e., flaws) in crystalline regions of RMS (Jane et al., 1997). For these reasons, the enzyme digested most parts of the remainder RMS much more quickly and even degraded part of the A-type crystallites in the second digestion phase. In addition, the C_{t2} results revealed that G50 contained more resistant starch than did RMS, which was consistent with previous research (Shrestha et al., 2012), as the existence of pores and crystallite "weak points" enhanced the accessibility of starch molecules to the amylase (i.e., reduced enzymatic resistance for RMS).

3.5 Digestion rate of alkali-treated starch

The above discussions have shown that compared to the increased treatment time, the increased alkali concentration was more effective at changing the multi-scale structure and thermal behavior of starch. Thus, the starches treated by the alkali solutions of both concentrations for 6 days were selected to further understand the effect of alkali on starch digestion rate. Fig. 5 shows the typical digestion curves, LOS plots and fit curves for alkali-treated RMS and G50; and Table 2 records the related parameters of digestion. Note that the residuals deduced from the fit data and digestion data (see Fig. S3) were in the range of -2~2, indicating that LOS model was capable of describing the starch digestion process accurately.

With alkali treatment at the low concentration (0.1%), the LOS plots retained two linear ranges (dual-phase digestion) for both starches. In the first phase, both alkali-treated RMS and G50 were digested at similar rates (k_1) ($P > 0.05$) but to higher extents (higher C_{t1}) than were their native

463 counterparts. It was possible that some parts in native starch with a lower digestion rate (k_2) were
464 transformed into materials with a higher digestion rate (k_1). The increases in C_{t1} were similar for two
465 starches, but still alkali-treated RMS had higher C_{t1} than alkali-treated G50. In the second phase, both
466 alkali-treated starches showed unchanged k_2 from those for their native counterparts.
467 Interestingly, when the alkali concentration was increased to 0.5%, a digestion course with three
468 different rates (with $k_1 > k_2 > k_3$, see Fig. 5 and Table 2) was employed to fit the digestion data instead of
469 dual-phase one (see Fig. S4), indicating that the treatment with high alkali concentration gave rise to a
470 triple-phase digestion pattern. Both RMS and G50 after the 0.5% alkali treatment showed higher k_1 and
471 C_{t1} than those with the 0.1% alkali treatment, suggesting enhanced digestibility. In addition, in all three
472 digestion phases, the high-concentration alkali-treated RMS showed higher digestion rates (k_1, k_2, and k_3)
473 and higher digested proportions (C_{t1}, C_{t2} and C_{t3}) than G50 treated under the same condition. In the
474 intermediate phase, 14% ($C_{t2} - C_{t1}$) of starch was digested for RMS and 9% ($C_{t2} - C_{t1}$) for G50.
475 Similar to the enzymatic hydrolysis procedure of starch, the treatment by alkali solution of starch
476 granules could act in several steps, including the penetration of alkali into the granules, the alkali-
477 induced disorganization in the multi-scale structure, and the out-phasing of starch molecules (especially
478 with low molecular weight) from the granules. The efficiency of alkali treatment at weakening starch
479 packing could be influenced by the porosity of starch granules. With pores in RMS granules, the alkali
480 solution could not only easily penetrate into the granules, inducing breakage of hydrogen bonding in the
481 hierarchical structure, but also enhance the leaching of starch molecules from the granule interior. For
482 G50, alkali treatment could only act through a “washing” procedure from the superficial regions of
483 granules, although the alkali solution might gradually diffuse into the granules at a rather slow rate. Thus,
484 “centrifugal” and “centripetal” alkali treatment manners existed for RMS and G50, respectively. Also,
485 RMS had the less-perfect A-type polymorph containing “weak point” (Jane et al., 1997) which was more
486 susceptible to alkali treatment (see Fig. 6).
487
488

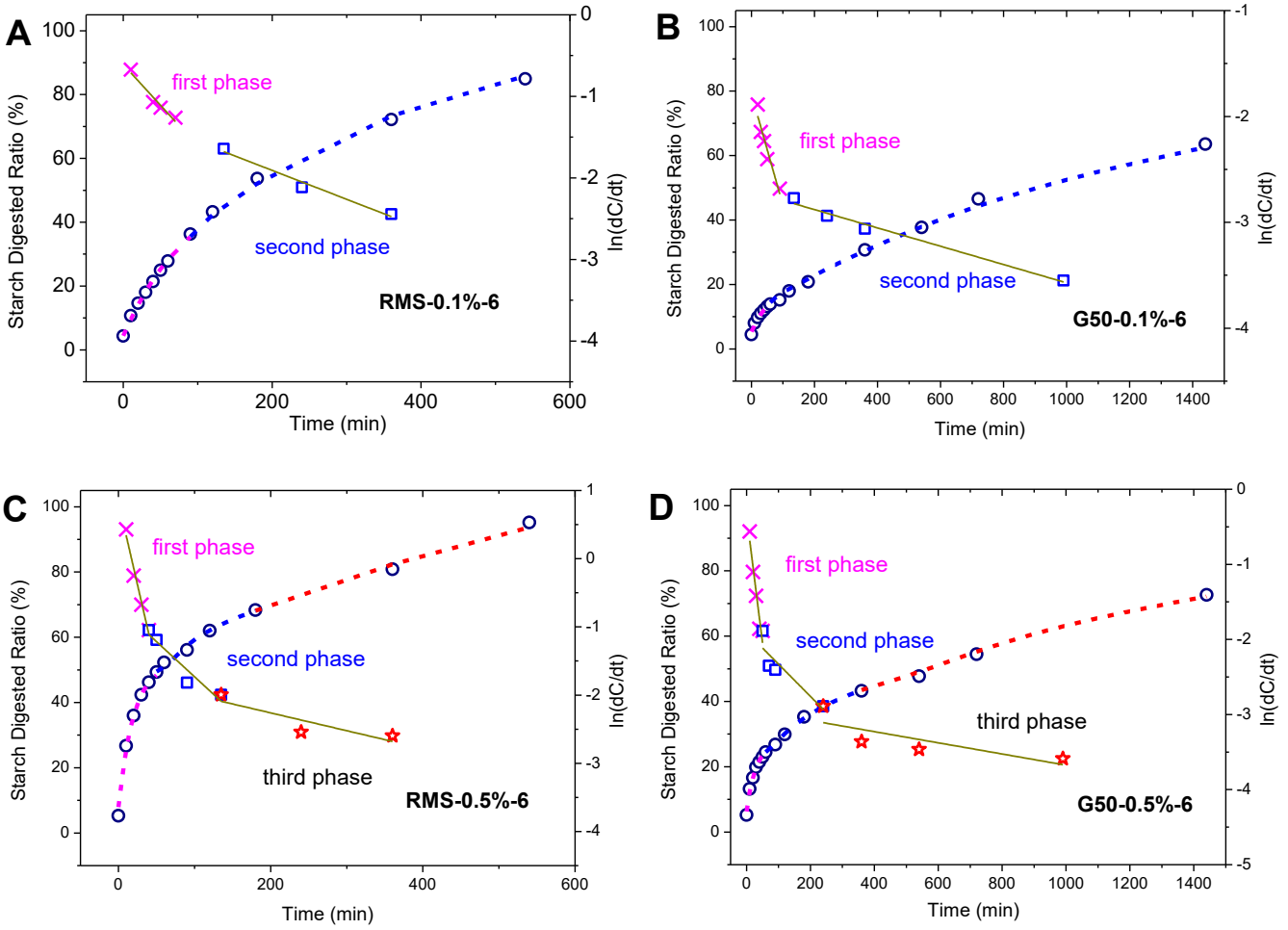

Fig. 5 Typical digestion curves, LOS plots and fit curves for alkali-treated RMS and G50. ○, Experiment data; ×, □ and ☆, LOS plot data in first, second and third phases, respectively; ——, linear fit curve for LOS plot data; , – – – – or, – – , fit curve based on the slope and intercept values of the linear fit curve for LOS plot in first, second and third phases, respectively.

Consequently, the alkali treatment at low (0.1%) concentration was capable of disorganizing the crystallites (decreased X_c) accompanied with increased thermal stability of the molecular order, and disrupting semi-crystalline lamellae. For both starches, the crystalline lamellae were swollen, as confirmed by increased d_c. This was because alkali treatment reduced the degree of alignment of double helices within lamellae. As the pores in RMS granules could facilitate the leaching of starch molecules from the granule interior, the alkali induced a reduction in the amorphous lamellar thickness of RMS

through the out-phasing of starch molecules from amorphous lamellae. However, G50 showed increased d_a (Fig. 1 and Table 1), as the out-phasing of starch molecules from amorphous lamellae might be greatly suppressed. Also, the compactness of amorphous materials, including amorphous lamellae and amorphous growth rings, could be reduced by alkali to a certain degree, as disclosed by SAXS. With weakened packing of starch structures on these different scales, some starch fractions (amorphous starch and crystallites with flaws) with a lower digestion rate (k_2) in the second phase was transformed into predominantly-amorphous starch with a higher digestion rate (k_1). Due to mild treatment by alkali solution (0.1% concentration), all these changes were relatively moderate. And eventually a modest increase in C_{t1} was observed for both starches, although they displayed almost unchanged digestion rates (k_1 and k_2) in both phases (Fig. 5 and Table 2).

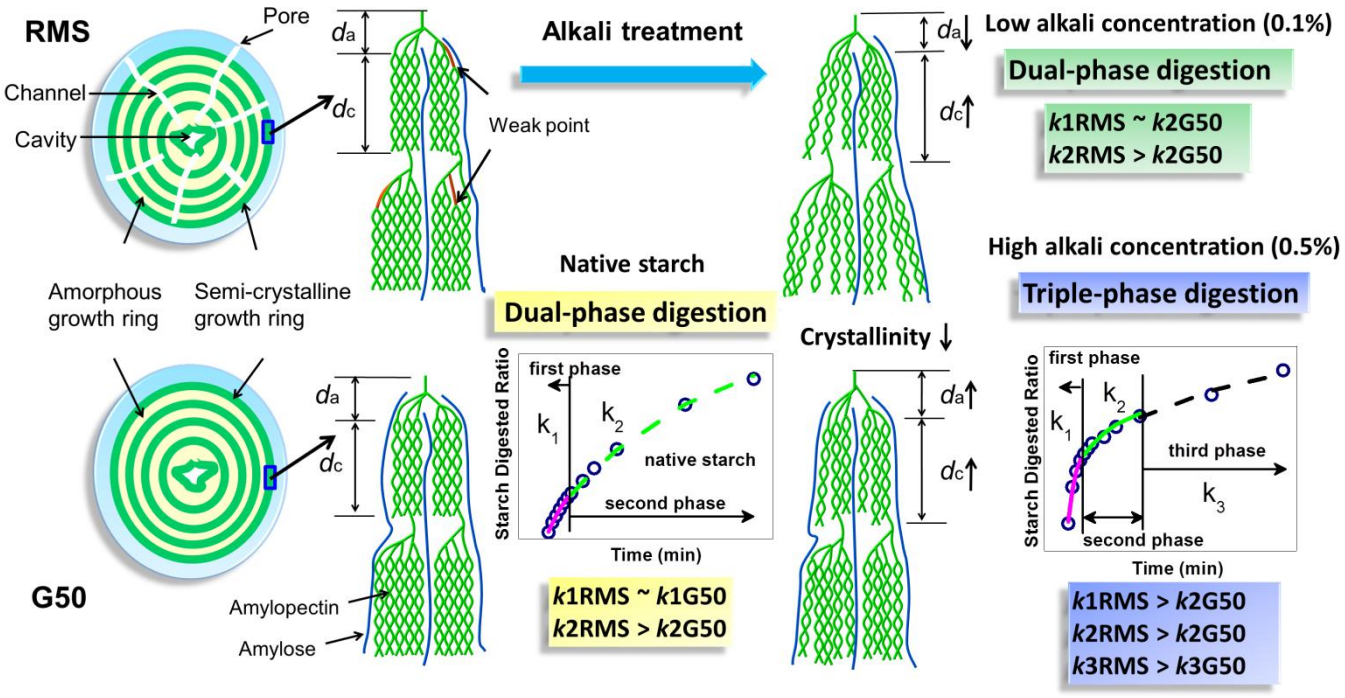

Fig. 6 Schematic representation for the differences of starch digestion processes of native and alkali-treated RMS and G50

However, when starch granules were treated by a stronger alkali solution (0.5% concentration), the reductions in starch molecular packing on multiple scales became more serious, contributing to the emergence of starch fractions with an intermediate digestion rate ($k_1 > k_2 > k_3$, see Fig. 5 and Table 2). For RMS, the treatment-induced structural changes were further facilitated by the pores and the flaws in A-type polymorphs. Thus, compared to G50, RMS displayed higher k_1 and k_2 in the first two phases respectively, as more prominently-weakened packing of RMS caused greater susceptibility of starch molecules to the enzyme.

4. Conclusion

In summary, native starches (RMS and G50) showed a dual-phase digestion behavior. Alkali treatment partially disorganized the crystallites and semi-crystalline lamellae, and reduced the packing compactness of starch amorphous materials (amorphous lamellae and amorphous growth rings). Consequently, partial starch was transformed into materials with a higher hydrolysis rate. The effect of alkali on starch were evidently enhanced by stronger alkali treatment (using an increased alkali concentration), resulting in the replacement of the dual-phase digestion by a triple-phase pattern, due to the emergence of a starch matrix with an intermediate hydrolysis rate. Furthermore, the multi-scale structural difference derived from the different amylose content determined the resistibility of starch to alkali treatment, eventually altering the digestion behavior. In particular, the pores and crystallite weak-points increased the susceptibility of starch granules to alkali treatment, resulting from an enhanced diffusion of alkali, which led to more prominent reduction of the packing of starch hierarchical structure (even the rupture of starch granules). This more apparently increased the digestion rate for RMS than for G50 under the same alkali treatment condition.

Therefore, from a hierarchical structural view, this work enables a comprehensive understanding of alkaline effects on the enzymatic digestion rate of starches with different amylose contents, which is of value for rational development of starchy foods with controlled digestibility and thus nutritional benefits

using alkali treatment. Again, since the main influences of alkali is to induce structural disorganizations for starch on different length scales, the results from present work are also valuable for design of starch-based food products with tailored digestion behavior, using other physicochemical treatments (plasma treatment, heat-moisture treatment, etc.) that tend to disorganize the hierarchical structure of starch products.

Abbreviations used:

RMS, regular maize starch; G50, Gelose 50 starch

Acknowledgments

The authors from SCUT, China would like to acknowledge research funds from National Natural Science Foundation of China (Nos. 31130042, 31571789) and Science and Technology Planning Project of Guangdong Province, China (Nos. B090600054, B010404002). The research is also supported by the Guangdong Innovative and Entrepreneurial Research Team Program (No. 2013C085). This research was partly undertaken on the SAXS/WAXS beamline at the Australian Synchrotron, Victoria, Australia. D. Qiao also would like to thank the China Scholarship Council (CSC) for providing research funding for his visiting studies at Monash University as part of her PhD work.

References

Aravind, N., Sissons, M., & Fellows, C. (2011). Can variation in durum wheat pasta protein and starch composition affect in vitro starch hydrolysis? *Food Chemistry, 124*(3), 816-821.

Blazek, J., & Gilbert, E. P. (2010). Effect of Enzymatic Hydrolysis on Native Starch Granule Structure. *Biomacromolecules, 11*(12), 3275-3289.

568 Butterworth, P. J., Warren, F. J., Grassby, T., Patel, H., & Ellis, P. R. (2012). Analysis of starch
569 amylolysis using plots for first-order kinetics. *Carbohydrate Polymers, 87*(3), 2189-2197.
570 Cai, J., Yang, Y., Man, J., Huang, J., Wang, Z., Zhang, C., Gu, M., Liu, Q., & Wei, C. (2014). Structural
571 and functional properties of alkali-treated high-amylose rice starch. *Food Chemistry, 145*, 245-
572 253.
573 Cameron, R. E., & Donald, A. M. (1992). A small-angle X-ray scattering study of the annealing and
574 gelatinization of starch. *Polymer, 33*(12), 2628-2635.
575 Cameron, R. E., & Donald, A. M. (1993a). A Small-Angle X-Ray-Scattering Study of Starch
576 Gelatinization in Excess and Limiting Water. *Journal of Polymer Science Part B-Polymer*
577 *Physics, 31*(9), 1197-1203.
578 Cameron, R. E., & Donald, A. M. (1993b). A Small-Angle X-Ray-Scattering Study of the Absorption of
579 Water into the Starch Granule. *Carbohydrate Research, 244*(2), 225-236.
580 Campus-Baypoli, O. N., Rosas-Burgos, E. C., Torres-Chavez, P. I., Ramírez-Wong, B., & Serna-
581 Saldivar, S. O. (1999). Physiochemical changes of starch during maize tortilla production.
582 *Starch-Starke, 51*(5), 173-176.
583 Cardoso, M. B., Putaux, J.-L., Samios, D., & da Silveira, N. P. (2007). Influence of alkali concentration
584 on the deproteinization and/or gelatinization of rice starch. *Carbohydrate Polymers, 70*(2), 160-
585 165.
586 Chen, P., Yu, L., Simon, G., Petinakis, E., Dean, K., & Chen, L. (2009). Morphologies and
587 microstructures of cornstarches with different amylose-amylopectin ratios studied by confocal
588 laser scanning microscope. *Journal of Cereal Science, 50*(2), 241-247.
589 Cooke, D., & Gidley, M. J. (1992). Loss of crystalline and molecular order during starch gelatinisation:
590 origin of the enthalpic transition. *Carbohydrate Research, 227*, 103-112.
591 Correia, P. R., & Beirão-da-Costa, M. L. (2012). Starch isolation from chestnut and acorn flours through
592 alkaline and enzymatic methods. *Food and Bioproducts Processing, 90*(2), 309-316.

Dhital, S., Butardo, V. M., Jobling, S. A., & Gidley, M. J. (2015). Rice starch granule amylolysis–Differentiating effects of particle size, morphology, thermal properties and crystalline polymorph. *Carbohydrate Polymers, 115*, 305-316.

Edwards, C. H., Warren, F. J., Milligan, P. J., Butterworth, P. J., & Ellis, P. R. (2014). A novel method for classifying starch digestion by modelling the amylolysis of plant foods using first-order enzyme kinetic principles. *Food & function, 5*(11), 2751-2758.

Englyst, H. N., Kingman, S., & Cummings, J. (1992). Classification and measurement of nutritionally important starch fractions. *European journal of clinical nutrition, 46*, S33-50.

Gallant, D., Bouchet, B., Buléon, A., & Pérez, S. (1992). Physical characteristics of starch granules and susceptibility to enzymatic degradation. *European Journal of Clinical Nutrition, 46*, S3-16.

Goñi, I., Garcia-Alonso, A., & Saura-Calixto, F. (1997). A starch hydrolysis procedure to estimate glycemic index. *Nutrition Research, 17*(3), 427-437.

Han, J.-A., & Lim, S.-T. (2004). Structural changes in corn starches during alkaline dissolution by vortexing. *Carbohydrate Polymers, 55*(2), 193-199.

Han, J. Y., & Tyler, R. T. (2003). Characterization of pea starches in the presence of alkali and borax. *Starch‐Stärke, 55*(10), 457-463.

Han, X. Z., & Hamaker, B. R. (2002). Partial Leaching of Granule‐Associated Proteins from Rice Starch during Alkaline Extraction and Subsequent Gelatinization. *Starch‐Stärke, 54*(10), 454-460.

Hizukuri, S. (1985). Relationship between the distribution of the chain length of amylopectin and the crystalline structure of starch granules. *Carbohydrate Research, 141*(2), 295-306.

Hoover, R. (2010). The impact of heat-moisture treatment on molecular structures and properties of starches isolated from different botanical sources. *Critical Reviews in Food Science and Nutrition, 50*(9), 835-847.

617 Jane, J.-l., Wong, K.-s., & McPherson, A. E. (1997). Branch-structure difference in starches of A-and B-
618 type X-ray patterns revealed by their Naegeli dextrins. *Carbohydrate Research, 300*(3), 219-227.
619 Jiang, Q., Gao, W., Li, X., Man, S., Shi, Y., Yang, Y., Huang, L., & Liu, C. (2014). Comparative
620 susceptibilities to alkali-treatment of A-, B-and C-type starches of Dioscorea zingiberensis,
621 Dioscorea persimilis and Dioscorea opposita. *Food Hydrocolloids, 39*, 286-294.
622 Karim, A., Nadiha, M., Chen, F., Phuah, Y., Chui, Y., & Fazilah, A. (2008). Pasting and retrogradation
623 properties of alkali-treated sago (Metroxylon sagu) starch. *Food Hydrocolloids, 22*(6), 1044-
624 1053.
625 Kim, H.-S., & Huber, K. C. (2010). Physicochemical properties and amylopectin fine structures of A-
626 and B-type granules of waxy and normal soft wheat starch. *Journal of Cereal Science, 51*(3),
627 256-264.
628 Lai, L., Karim, A. A., Norziah, M., & Seow, C. (2002). Effects of Na_2CO_3 and NaOH on DSC thermal
629 profiles of selected native cereal starches. *Food Chemistry, 78*(3), 355-362.
630 Liu, H., Yu, L., Xie, F., & Chen, L. (2006). Gelatinization of cornstarch with different
631 amylose/amylopectin content. *Carbohydrate Polymers, 65*(3), 357-363.
632 Lopez-Rubio, A., Htoon, A., & Gilbert, E. P. (2007). Influence of extrusion and digestion on the
633 nanostructure of high-amylose maize starch. *Biomacromolecules, 8*(5), 1564-1572.
634 Manners, D. J. (1989). Recent developments in our understanding of amylopectin structure.
635 *Carbohydrate Polymers, 11*(2), 87-112.
636 McDougall, G. J., Shpiro, F., Dobson, P., Smith, P., Blake, A., & Stewart, D. (2005). Different
637 polyphenolic components of soft fruits inhibit α-amylase and α-glucosidase. *Journal of*
638 *Agricultural and Food Chemistry, 53*(7), 2760-2766.
639 Nadiha, M. N., Fazilah, A., Bhat, R., & Karim, A. A. (2010). Comparative susceptibilities of sago,
640 potato and corn starches to alkali treatment. *Food Chemistry, 121*(4), 1053-1059.
641 Nor Nadiha, M. Z., Fazilah, A., Bhat, R., & Karim, A. A. (2010). Comparative susceptibilities of sago,
642 potato and corn starches to alkali treatment. *Food Chemistry, 121*(4), 1053-1059.

643 Nwosu, F., Morris, J., Lund, V. A., Stewart, D., Ross, H. A., & McDougall, G. J. (2011). Anti-
644 proliferative and potential anti-diabetic effects of phenolic-rich extracts from edible marine algae.
645 *Food Chemistry, 126*(3), 1006-1012.
646 Paredes-Lópezb, O., & Bello-Péreza, L. A. (2007). Physicochemical and morphological characteristics
647 of nixtamalized maize starch. *Starch/Stärke, 59*, 277-283.
648 Payan, F., Haser, R., Pierrot, M., Frey, M., Astier, J., Abadie, B., Duée, B., & Buisson, G. (1980). The
649 three-dimensional structure of α-amylase from porcine pancreas at 5 Å resolution–The active-site
650 location. *Acta Crystallographica Section B: Structural Crystallography and Crystal Chemistry*,
651 *36*(2), 416-421.
652 Perez, S., & Bertoft, E. (2010). The molecular structures of starch components and their contribution to
653 the architecture of starch granules: A comprehensive review. *Starch-Starke*, *62*(8), 389-420.
654 Pikus, S. (2005). Small-angle x-ray scattering (SAXS) studies of the structure of starch and starch
655 products. *Fibres & Textiles in Eastern Europe, 13*(5), 82-86.
656 Poulsen, B. R., Ruiter, G., Visser, J., & Iversen, J. J. L. (2003). Determination of first order rate
657 constants by natural logarithm of the slope plot exemplified by analysis of Aspergillus niger in
658 batch culture. *Biotechnology Letters, 25*(7), 565-571.
659 Praznik, W., Buksa, K., Ziobro, R., Gambuś, H., & Nowotna, A. (2012). The effect of long‐term alkali
660 treatment on the molecular characteristics of native and extruded starches at 35° C. *Starch‐*
661 *Stärke, 64*(11), 890-897.
662 Russell, P. L. (1987). Gelatinisation of starches of different amylose/amylopectin content. A study by
663 differential scanning calorimetry. *Journal of Cereal Science, 6*(2), 133-145.
664 Shiau, S.-Y., & Yeh, A.-I. (2001). Effects of alkali and acid on dough rheological properties and
665 characteristics of extruded noodles. *Journal of Cereal Science, 33*(1), 27-37.

Shrestha, A. K., Blazek, J., Flanagan, B. M., Dhital, S., Larroque, O., Morell, M. K., Gilbert, E. P., & Gidley, M. J. (2012). Molecular, mesoscopic and microscopic structure evolution during amylase digestion of maize starch granules. *Carbohydrate Polymers, 90*(1), 23-33.

Tan, I., Flanagan, B. M., Halley, P. J., Whittaker, A. K., & Gidley, M. J. (2007). A method for estimating the nature and relative proportions of amorphous, single, and double-helical components in starch granules by C-13 CP/MAS NMR. *Biomacromolecules, 8*(3), 885-891.

Thys, R. C., Westfahl Jr, H., Noreña, C. P., Marczak, L. D., Silveira, N. P., & Cardoso, M. B. (2008). Effect of the alkaline treatment on the ultrastructure of C-type starch granules. *Biomacromolecules, 9*(7), 1894-1901.

Wang, B., Li, D., Wang, L.-j., Liu, Y.-h., & Adhikari, B. (2012). Effect of high-pressure homogenization on microstructure and rheological properties of alkali-treated high-amylose maize starch. *Journal of Food Engineering, 113*(1), 61-68.

Wang, S., & Copeland, L. (2012). Effect of alkali treatment on structure and function of pea starch granules. *Food Chemistry, 135*(3), 1635-1642.

Wang, S., Luo, H., Zhang, J., Zhang, Y., He, Z., & Wang, S. (2014). Alkali-induced changes in functional properties and in vitro digestibility of wheat starch: The role of surface proteins and lipids. *Journal of Agricultural and Food Chemistry, 62*(16), 3636-3643.

Zhang, B., Chen, L., Xie, F., Li, X., Truss, R. W., Halley, P. J., Shamshina, J. L., Rogers, R. D., & McNally, T. (2015). Understanding the structural disorganization of starch in water-ionic liquid solutions. *Physical Chemistry Chemical Physics, 17*, 13860-13871.

Zhang, B. J., Li, X. X., Liu, J., Xie, F. W., & Chen, L. (2013). Supramolecular structure of A- and B-type granules of wheat starch. *Food Hydrocolloids, 31*(1), 68-73.

Zhang, B. J., Zhao, Y., Li, X. X., Li, L., Xie, F. W., & Chen, L. (2014a). Supramolecular structural changes of waxy and high-amylose cornstarches heated in abundant water. *Food Hydrocolloids, 35*, 700-709.

Zhang, B. J., Zhao, Y., Li, X. X., Zhang, P. F., Li, L., Xie, F. W., & Chen, L. (2014b). Effects of amylose and phosphate monoester on aggregation structures of heat-moisture treated potato starches. *Carbohydrate Polymers, 103*, 228-233.

Zhang, G., Ao, Z., & Hamaker, B. R. (2006). Slow digestion property of native cereal starches. *Biomacromolecules, 7*(11), 3252-3258.

Zou, W., Sissons, M., Gidley, M. J., Gilbert, R. G., & Warren, F. J. (2015). Combined techniques for characterising pasta structure reveals how the gluten network slows enzymic digestion rate. *Food Chemistry, 188*, 559-568.

Figure captions

Fig. 1 SAXS patterns for native and alkali-treated RMS and G50.

Fig. 2 XRD patterns for native and alkali-treated RMS and G50.

Fig. 3 DSC thermograms for native and alkali-treated RMS and G50.

Fig. 4 Typical digestion curves, LOS plots and fit curves for native RMS and G50. ○, Experiment data; × and □, LOS plot data in first and second phases, respectively; ——, linear fit curve for LOS plot data; – – and – – , fit curve based on the slope and intercept values of the linear fit curve for LOS plot in first and second phases, respectively.

Fig. 5 Typical digestion curves, LOS plots and fit curves for alkali-treated RMS and G50. ○, Experiment data; ×, □ and ☆, LOS plot data in first, second and third phases, respectively; ——, linear fit curve for LOS plot data; , – – – – or, – – , fit curve based on the slope and intercept values of the linear fit curve for LOS plot in first, second and third phases, respectively.

Fig. 6 Schematic representation for the differences of starch digestion processes of native and alkali-treated RMS and G50.

Insights into the hierarchical structure and digestion rate of alkali-modulated starches with different amylose contents

Dongling Qiao[1,2,3], Long Yu[1,2*], Hongsheng Liu[1], Wei Zou[4], Fengwei Xie[5,6**], George Simon[2], Eustathios Petinakis[3], Zhiqi Shen[3], Ling Chen[1]

[1] CPFRR, College of Food Science and Engineering, South China University of Technology, Guangzhou, Guangdong 510640, China

[2] Department of Materials Engineering, Monash University, Melbourne, Vic 3168, Australia

[3] CSIRO, Manufacturing, Melbourne, Vic 3168, Australia

[4] Centre for Nutrition and Food Sciences, Queensland Alliance for Agriculture and Food Innovation, The University of Queensland, Brisbane, Qld 4072, Australia

[5] Australian Institute for Bioengineering and Nanotechnology, The University of Queensland, Brisbane, Qld 4072, Australia

[6] School of Chemical Engineering, The University of Queensland, Brisbane, Qld 4072, Australia

SUPPLMENTARY DATA

2500 ×

20000 ×

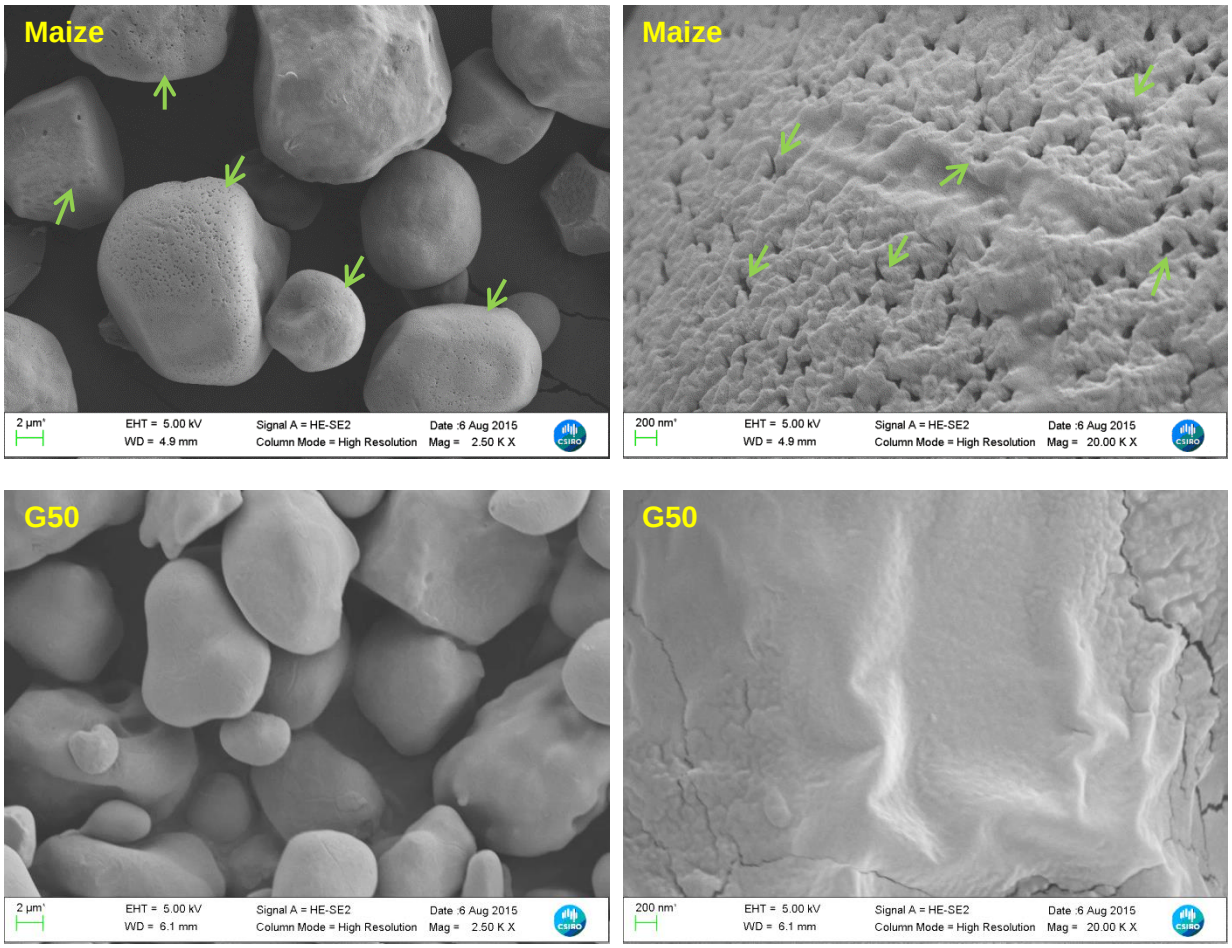

Fig. S1 SEM images of RMS and G50 observed at 2500 × and 20000 × magnifications. The green arrows indicate the pinholes of starch granules.

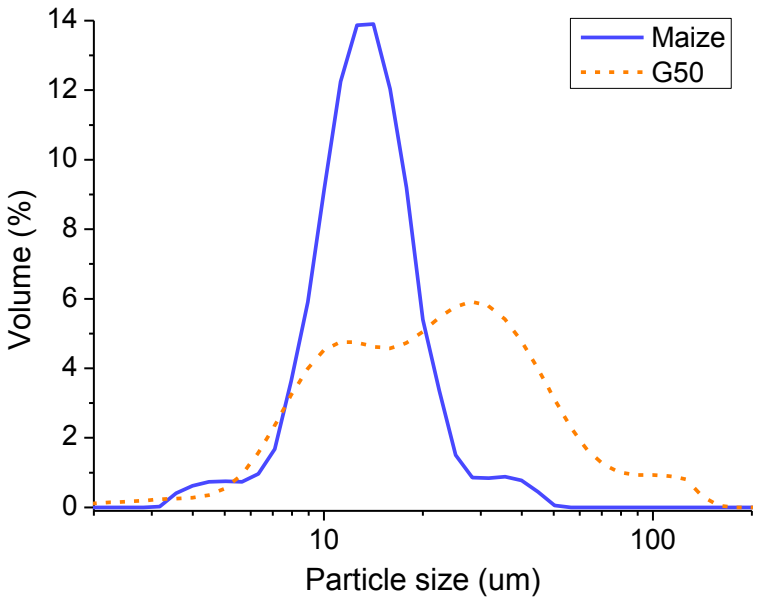

Fig. S2 Granule size distributions of native RMS and G50.

Table S1. Least Significant Difference analysis of starch digestion rate constants (k, min^{-1}) of RMS and alkali-treated RMS.

		RMS		RMS-0.1%-6		RMS-0.5%-6		
		k_1	k_2	k_1	k_2	k_1	k_2	k_3
RMS	k_1		0.000	0.672	0.000	0.000	0.235	0.000
	k_2	0.000		0.000	0.958	0.000	0.000	0.672
RMS-0.1%-6	k_1	0.672	0.000		0.000	0.000	0.432	0.000
	k_2	0.000	0.958	0.000		0.000	0.000	0.711
RMS-0.5%-6	k_1	0.000	0.000	0.000	0.000		0.000	0.000
	k_2	0.235	0.000	0.432	0.000	0.000		0.000
	k_3	0.000	0.672	0.000	0.711	0.000	0.000	

Table S2. Least Significant Difference analysis of starch digestion rate constants (k, min^{-1}) of G50 and alkali-treated G50.

		G50		G50-0.1%-6		G50-0.5%-6		
		k_1	k_2	k_1	k_2	k_1	k_2	k_3
G50	k_1		0.000	0.598	0.000	0.000	0.000	0.000
	k_2	0.000		0.000	0.832	0.000	0.001	0.958
G50-0.1%-6	k_1	0.598	0.000		0.000	0.000	0.000	0.000
	k_2	0.000	0.832	0.000		0.000	0.002	0.874
G50-0.5%-6	k_1	0.000	0.000	0.000	0.000		0.000	0.000
	k_2	0.000	0.001	0.000	0.002	0.000		0.001
	k_3	0.000	0.958	0.000	0.874	0.000	0.001	

Table S3. Coefficients of determination for starch digestion rate constants (k, min^{-1}) of G50 and alkali-treated G50.

R^2	RMS		RMS-0.1%-6		RMS-0.5%-6		G50		G50-0.1%-6		G50-0.5%-6	
k_1	0.972	0.895	0.957	0.812	0.980	0.984	0.877	0.963	0.927	0.970	0.864	0.941
k_2	0.995	0.985	0.969	0.989	0.922	0.976	0.842	0.897	0.985	0.834	0.982	0.820
k_3	--	--	--	--	0.784	0.785	--	--	--	--	0.933	0.792

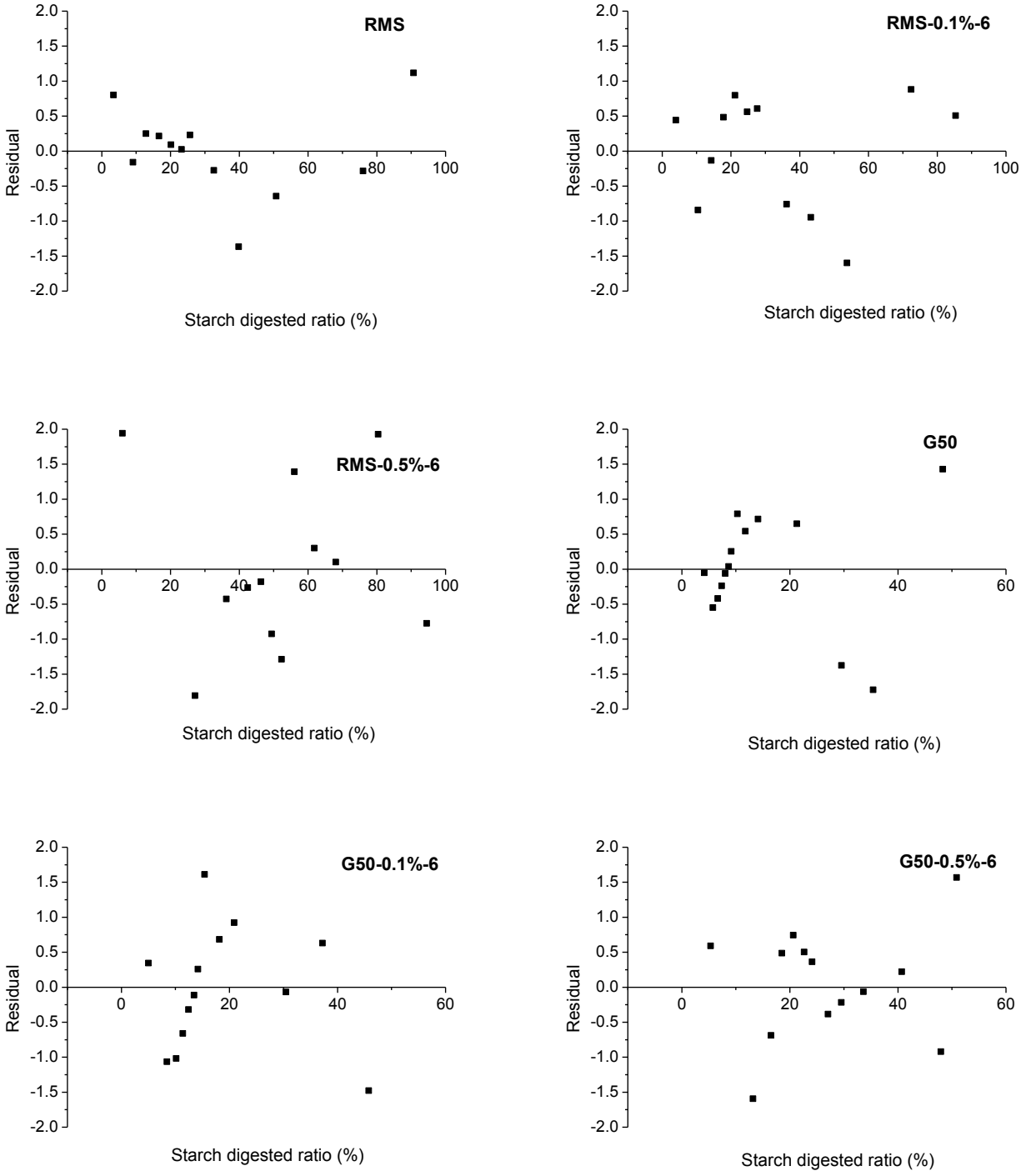

Fig. S3. Residual plots of LOS model for native and alkali-treated RMS and G50.

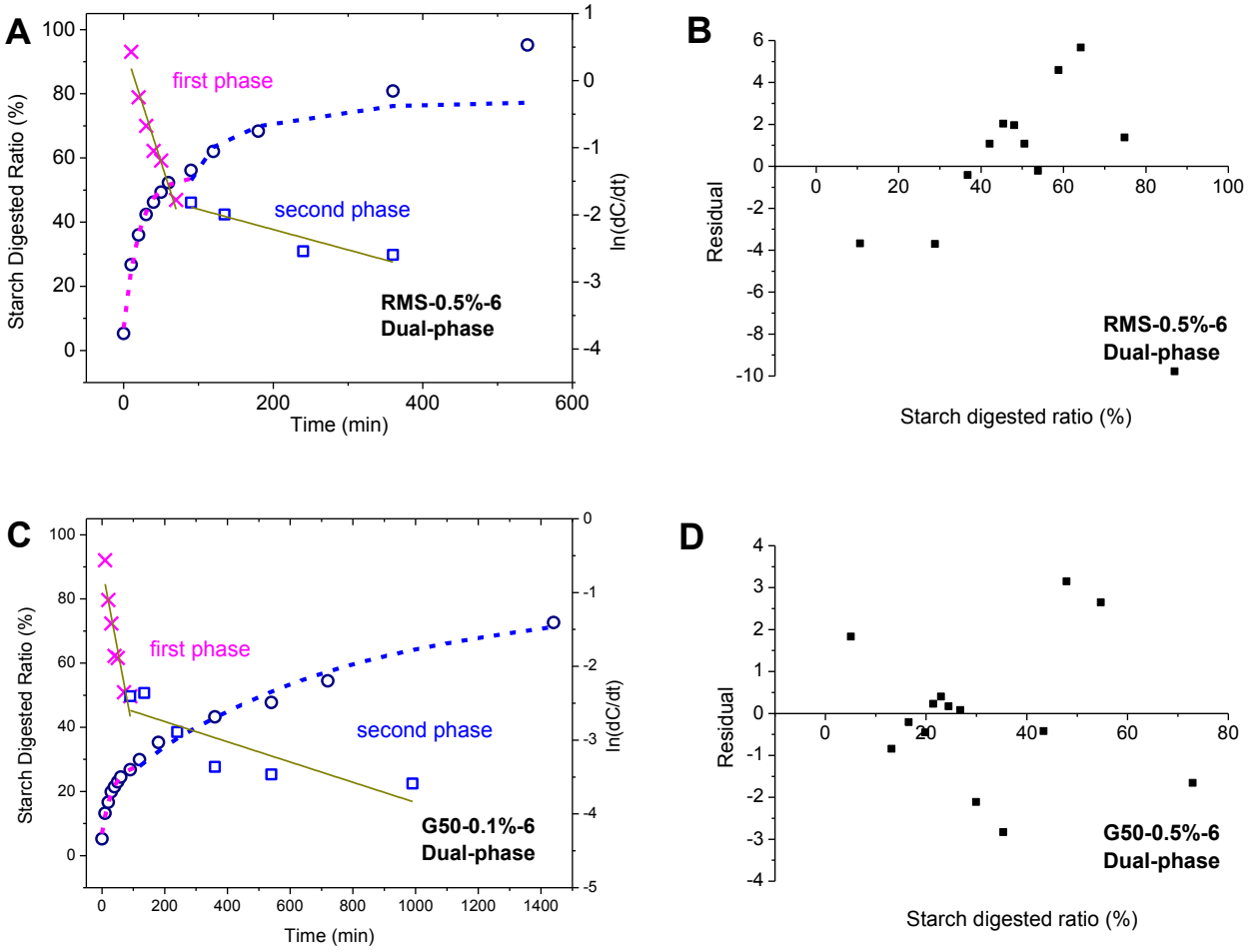

Fig. S4. Dual-phase digestion curves, LOS plots and fit curves for RMS-0.5%-6 (A) and G50-0.5%-6 (C), and their corresponding residual plots (B and D). ○, Experiment data; × and □, LOS plot data in first and second phases, respectively; ——, linear fit curve for LOS plot data; —— and – – , fit curves based on the slope and intercept values of the linear fit curves for the LOS plots in first and second phases, respectively.